coatings

MDPI

Article

MnO_2/Carbon Nanofibers Material as High-Performance Anode for Lithium-Ion Batteries

Dandan Ma [1,2], Xin Mu [1], Guiqing Zhao [1], Xiangge Qin [1,*] and Meili Qi [1,*]

[1] School of Materials Science and Engineering, Jiamusi University, Jiamusi 154007, China; mxstc68@foxmail.com (X.M.)
[2] School of Information Science and Electronic Technology, Jiamusi University, Jiamusi 154007, China
* Correspondence: qinxiangge@jmsu.edu.cn (X.Q.); meili8585@foxmail.com (M.Q.); Tel.: +86-0454-8618-703 (X.Q.)

Abstract: MnO_2 has advantages such as the simple and diverse preparation methods, low cost and high theoretical capacity, but its industrial application is affected by its poor conductivity and fast attenuation of cycle performance. In order to improve its conductivity, battery capacity and performance, MnO_2/carbon nanofibers (MnO_2/CNFs) are obtained by using electrospinning technology, and the electrochemical performance was confirmed by XRD, SEM, TEM. Confirmed by comparison, the 20% MnO_2/CNFs exhibit superior and excellent long cycling performance with a reversible capacity of 835 mA h g^{-1} at 0.1 A g^{-1} after the 133th cycle and a high initial specific capacity of 1094 mA h g^{-1} at a current density of 0.1 A g^{-1}. The MnO_2/CNFs have notable specific capacities with a coulombic efficiency of 99.5%, which greatly improve the reaction rate. This can also be used as a flexible electrode material because of its good flexibility. Due to the fact that carbon has better electron/ion conductivity, it shows better kinetics.

Keywords: lithium-ion batteries; carbon nanofibers; MnO_2; the anode material

check for updates

Citation: Ma, D.; Mu, X.; Zhao, G.; Qin, X.; Qi, M. MnO_2/Carbon Nanofibers Material as High-Performance Anode for Lithium-Ion Batteries. *Coatings* **2023**, *13*, 707. https://doi.org/10.3390/coatings13040707

Academic Editor: Torsten Brezesinski

Received: 17 March 2023
Revised: 28 March 2023
Accepted: 29 March 2023
Published: 31 March 2023

Copyright: © 2023 by the authors. Licensee MDPI, Basel, Switzerland. This article is an open access article distributed under the terms and conditions of the Creative Commons Attribution (CC BY) license (https://creativecommons.org/licenses/by/4.0/).

1. Introduction

Anode material is one of the core materials of a battery. It is an important factor in determining the safety, cycling stability and other performance of battery [1–3]. The development of high-capacity anode materials is very important to further improve the energy density of Li-ion batteries [4–6]. With unique outer valence electrons and special physical and chemical properties, transition metal manganese compounds are one of the high-capacity lithium-ion anode materials that have attracted more attention in recent years [7], among which MnO_2 is viewed as one of the most valuable electrode materials for lithium battery due to its advantages such as simple and diverse preparation methods, low cost and high capacity (theoretical capacity is 1232 mA h g^{-1}) [8,9]. However, MnO_2 also has some disadvantages, involving volume change during the repeated process of charge/discharge and poor electrical conductivity, which result in poor performance of rate and inferior stability of cycle [10–12].

To solve the problems and improve the electrochemical performance, many effective strategies have been researched, such as materials, porous structure, and conductive polymer/metallic material coating [13–16]. Recently, significant effort has been devoted to nanowires, nanosheets, and porous nanostructures to boost the lithium-ion concentration [17–19]. Sui et al. synthesized semiconducting polypyrrole coated-δ-MnO_2 nanosheet arrays on nickel foam by hydrothermal and electro-deposition. Coated-δ-MnO_2 nanosheet arrays can afford ~430 mA h g^{-1} after 120 cycles [20]. Single crystalline α-MnO_2 nanowires, investigated by Ahmad Umar et al., provide a stable capacity of 330 mA h g^{-1} for 60 cycles [21]. Special nanostructures have high specific surface area and a great number of active sites, which could enhance electrochemical performance [22,23]. However, because these designs could buffer the anode material of lithium-ion batteries, it is difficult

to apply this design directly to the anode material of lithium-ion batteries and the cyclic stability of the anode material is still not ideal. This is because the electrical conductivity of MnO_2 is poor, which causes larger volume expansion. Therefore, it is necessary to design a unique anode of lithium-ion battery [24–26]. The embedding of MnO_2 nanoparticles into carbon nanofibers (CNFS) as independent substrates by electrospinning has been extensively studied, but there has been little research on the embedding of MnO_2 nanotubes into carbon nanofibers as independent electrodes.

Herein, MnO_2/carbon nanofibers (MnO_2/CNFs) were designed by electrospinning technology to enhance the electrochemical properties. This design has several advantages. Firstly, it effectively improves the conductivity and limits the volume expansion, which ensures the stability of the electrode during electrochemical cycling [27,28]. Secondly, MnO_2/CNFs has large specific surface area and high porosity, which can improve the adsorption, catalysis and transfer properties of the material [29,30]. Thirdly, the fracture strength and elastic modulus of the fiber are significantly improved, and it has good flexibility, which can be used as the precursor of flexible materials [31,32]. The results show that MnO_2/CNFs exhibit superior storage behavior and excellent long cycling performance with a reversible capacity of 835 mA h g^{-1} at 0.1 A g^{-1} after the 133th cycle. MnO_2/CNFs exhibit notable specific capacities with a coulombic efficiency of 99.5%, which greatly improves the reaction rate and shows better kinetics due to the fact that carbon has better electron/ion conductivity.

2. Experimental Section

2.1. Preparation of MnO_2

The transition metal Oxide MnO_2 was prepared by hydrothermal method. Firstly, 0.2 g $KMnO_4$ was mixed with 25 mL H_2O and stirred for 10 min. Then, 1.25 mL HNO_3 was added, stirred thoroughly, and transferred into a 50 mL Teflon lined stainless steel reactor for hydrothermal reaction at 120 °C for 12 h, cooling naturally. Centrifugal washing was performed at 10,000 rates, then drying. MnO_2 powder was prepared.

2.2. Preparation of MnO_2 NTs

MnO_2 was calcined to produce MnO_2 NTs. MnO_2 powder was put into a tubular furnace and heat treatment was applied in 400 °C air for 4 h to obtain MnO_2 NTs.

2.3. Preparation of MnO_2 Nanofibers (NFs)

The polymer containing 5% MnO_2 NFs and 20% MnO_2 NFs was prepared by electrospinning. Weighed out required amounts of MnO_2 NTs, N, N dimethylformamide (Tianjin Kaitong Chemical Reagent Co., Ltd., Tianjin, China) were mixed, put in the ultrasonic cleaning machine until fully dissolved, then the appropriate amount of polyacrylonitrile (PAN) was added. The mixture was continuously put in the ultrasonic cleaning machine until all was dissolved. Then, it was mixed into the required slurry in the electrostatic spinning machine for spinning. After re-coating by electrospinning, the polymer containing 5% MnO_2/NFs and 20% MnO_2/NFs was prepared.

2.4. Preparation of MnO_2/CNFs

MnO_2 NFs polymer was calcined to produce MnO_2/CNFs. First, 5% MnO_2 /NFs polymer and 20% MnO_2/NFs polymer were placed in tubular furnace, respectively, and carbonized in Ar atmosphere at 600 °C for 4 h to obtain 5% MnO_2/CNFs and 20% MnO_2/CNFs. Schematic of the synthesis procedure of MnO_2/CNFs is provided in Figure 1.

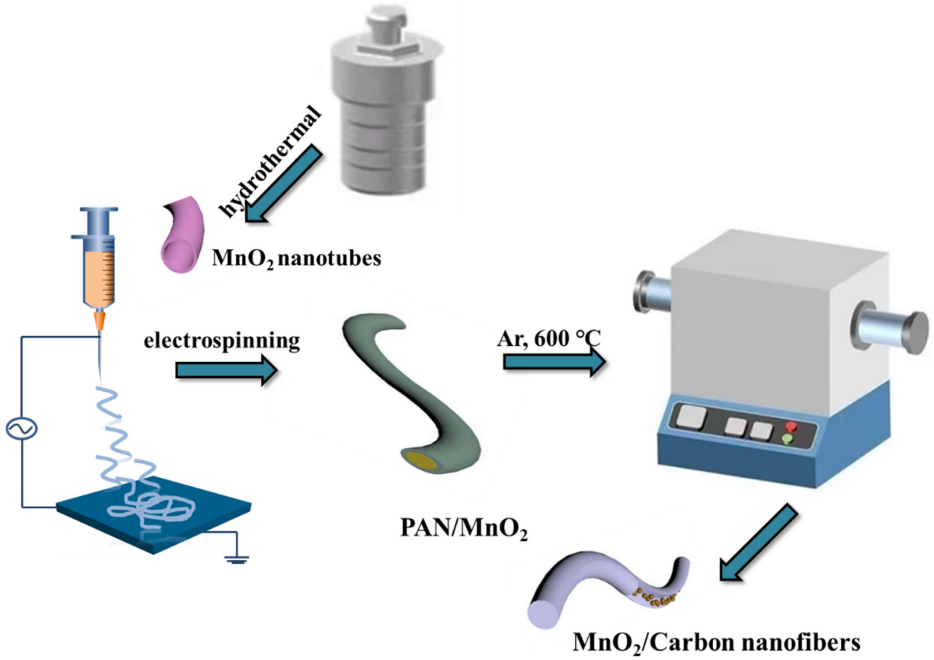


Figure 1. Schematic of the synthesis procedure of the MnO_2/Carbon nanofibers.

2.5. Material Characterization

The compositions of MnO_2 NTs, 5% MnO_2/CNFs and 20% MnO_2/CNFs were characterized by X-ray diffraction (XRD, D8Advance, Bruker AXS, Karlsruhe, Germany), scanning electron microscope (SEM, JSM-6360LV, JEOL, Tokyo, Japan) and transmission electron microscope (TEM, Fei Tecnai G2 F20S-Twin, Hillsboro, OR, USA), then the morphology was further observed. The batteries were assembled in the glove box using 5% MnO_2/CNFs and 20% MnO_2/CNFs as anode materials, and dried at room temperature for 24 h.

3. Results and Discussion

3.1. Morphology and Structure

The morphologies and structures of MnO_2 NTs, 5% MnO_2/CNFs and 20% MnO_2/CNFs were obtained. Figure 2 characterizes the morphology of MnO_2 NTs by scanning electron microscopy (SEM) at different magnifications. Figure 2a displays the tubular structure of MnO_2 NTs with the longest morphology of about 3.3 µm. The morphologies of MnO_2 NTs have better uniformity and contain almost no impurity particles. As shown in Figure 3b, hollow tubes are gained with an average diameter of 100 nm (±100). Figure 3a,b shows the 5% MnO_2/CNFs, and Figure 3c,d shows the 20% MnO_2/CNFs; both of them are uniform nanofibers with a diameter of approximately 300–500 nm. Their uniformly distributed nanoparticles are in high concentration, which reveals that the uniform MnO_2/CNFs can be prepared [33,34].

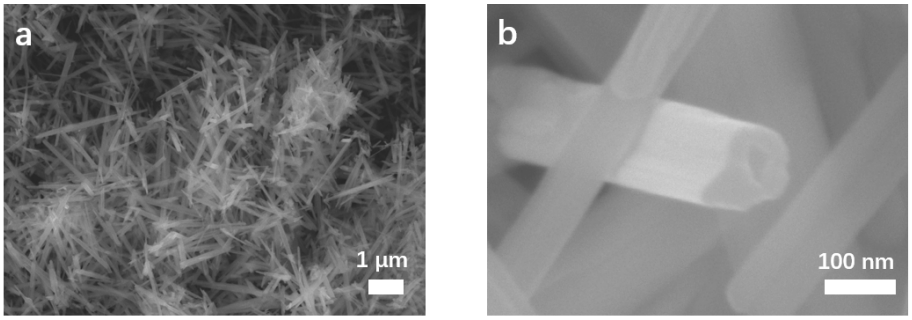


Figure 2. SEM images of MnO_2 NTs (**a**,**b**).

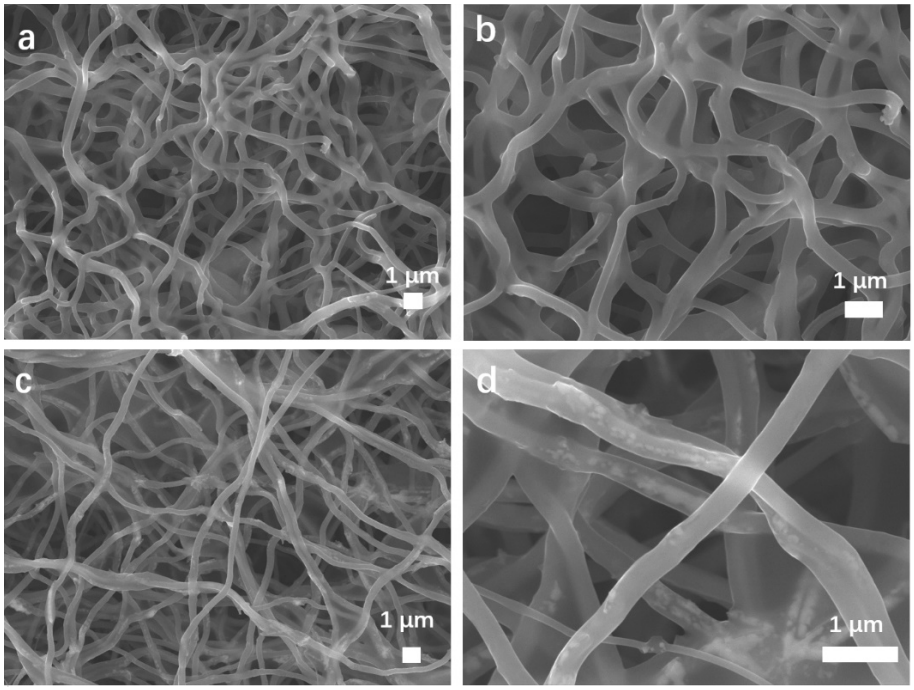


Figure 3. SEM images of the MnO_2/CNFs in different components: 5% MnO_2/CNFs (**a**,**b**); 20% MnO_2/CNFs (**c**,**d**).

The crystal structures and phase information of MnO_2 NTs, 5% MnO_2/CNFs and 20% MnO_2/CNFs were characterized by X-ray diffraction (XRD). The results are demonstrated in Figure 4. The diffraction peaks of MnO_2 NTs, 5% MnO_2/CNFs and 20% MnO_2/CNFs are in line with the standard card of MnO_2 (JCPDS NO. 44-0141). The XRD patterns of MnO_2 NTs, 5% MnO_2/CNFs and 20% MnO_2/CNFs show no noticeable change. The typical diffraction peaks correspond to the (110), (200), (220), (310), (211), (301), (411), (431), (521), (002), (541), (312) and (332) crystal planes of manganese dioxide, respectively. This indicates that manganese dioxide was integrated into the composite material, which presents the successful preparation. The peak of 20% MnO_2/CNFs is strong and narrow, which confirms good crystallinity and high purity [35,36].

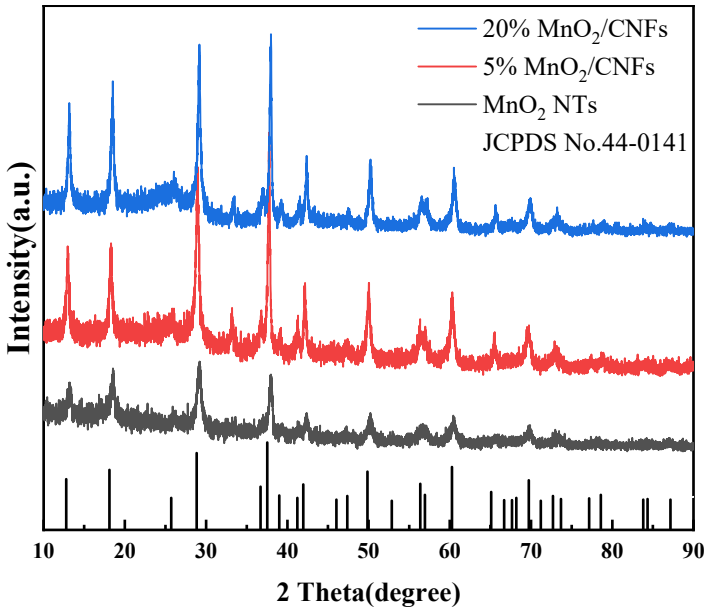


Figure 4. XRD patterns of MnO_2 NTs, 5% MnO_2/CNFs and 20% MnO_2/CNFs.

To further study the structure of 20% MnO_2/CNFs samples, the TEM characterization is shown in Figure 5. The prepared 20% MnO_2/CNFs showed a nanotube structure with the diameter of 250 nm and filled with the MnO_2 particles in Figure 5b. In Figure 5c, the high-resolution TEM image of the MnO_2/CNFs demonstrates that the lattice spacings are 0.182 and 0.161 nm, which is in line with the spacing of the (411) and (431) planes of MnO_2. Obviously, it is proved that the ingredient of the nanofibers is MnO_2 again [19,36,37].

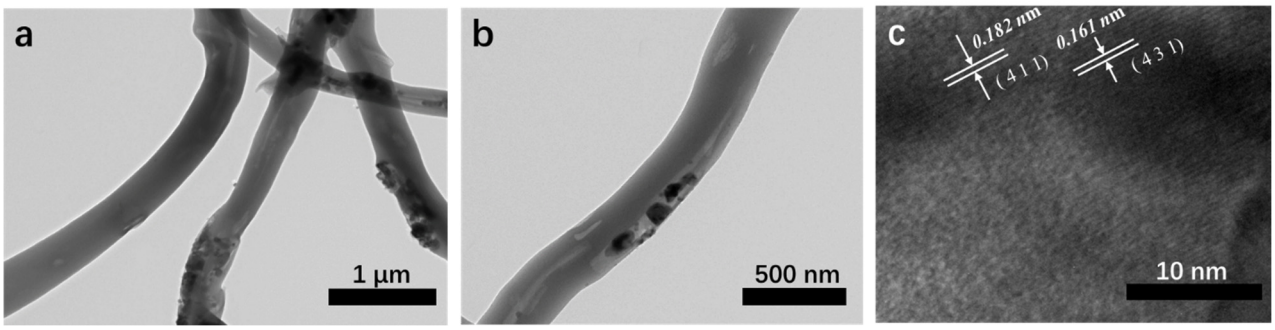


Figure 5. TEM images of 20% MnO_2/CNFs (**a**,**b**) and HRTEM image of 20% MnO_2/CNFs (**c**).

3.2. Electrochemical Performance

The lithium electrochemical performances of MnO_2 NTs, 5% MnO_2/CNFs and 20% MnO_2/CNFs were evaluated using coin cells. The CV curves of MnO_2 NTs, 5% MnO_2/CNFs and 20% MnO_2/CNFs for the first several cycles at a scan rate of 0.1 mV s^{-1} in the potential range 0.01–3.0 V are shown, respectively, in Figure 6a–c. Compared with MnO_2 NTs and 5% MnO_2/CNFs in Figure 6a,b, the first cathodic cycle creates a broad peak at 0.45 V in Figure 6c, which vanishes in the following cathodic cycles. This illustrates that the reaction is irreversible and the energy difference prompts the formation of the solid electrolyte interface (SEI) on the electrode surface [30,31]. In addition to this, the peak decreases sharply below 0.35 V. This occurs because of the reduction in Mn^{4+} to Mn^0 ($MnO_2 + 4Li^+ + 4e^- \rightarrow Mn + 2Li_2O$) [22,38]. In the first anodic cycles, the strong peak at 1.32 V is corresponding to the dissolution of Li^+ from Li_2O and the oxication of Mn^0 to Mn^{2+} ($Mn + 2Li_2O \rightarrow MnO_2 + 4Li^+ + 4e^-$) [22,23,38]. In the other anodic cycles, the reaction is reversible because the peaks have no obvious changes. In addition, almost in the same place, the excellent electrochemical stability was revealed.

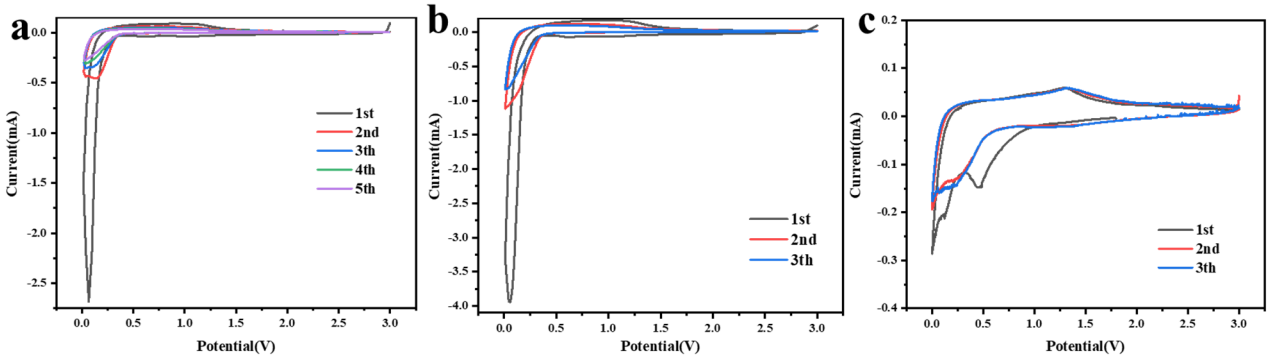


Figure 6. Cyclic voltammetry curves of MnO_2 NTs. (**a**) 5% MnO_2/CNFs (**b**) and 20% MnO_2/CNFs (**c**) at a scan rate of 0.1 mV s^{-1} in the potential range of 0.01–3.0 V.

The discharge/charge graphs of 5% MnO_2/CNFs and 20% MnO_2/CNFs at a current density of 0.1 A g^{-1} are displayed in Figure 7a,b. The curves of lap 1, lap 20 and lap 50 were regarded as the samples There are obvious discharge voltage plateaus at about 0.76 V (Figure 7a) and 0.57 V (Figure 7b). The specific capacities of the first discharge are 1023 and 1094 mA h g^{-1}, respectively; in the following cycles, the specific capacities are around 531–558 and 658–704 mA h g^{-1}. An SEI film was formed due to the lost capacity, which

is irreversible, and it is the same as cyclic voltammetry curves (Figure 7a,b). Thus, the mechanism of alloying lithiation is proved. Meanwhile, the discharge/charge capacity of the 20% MnO_2/CNFs remains higher than that of the 5% MnO_2/CNFs, which indicates not only high performance, but also excellent battery reversibility [39,40].

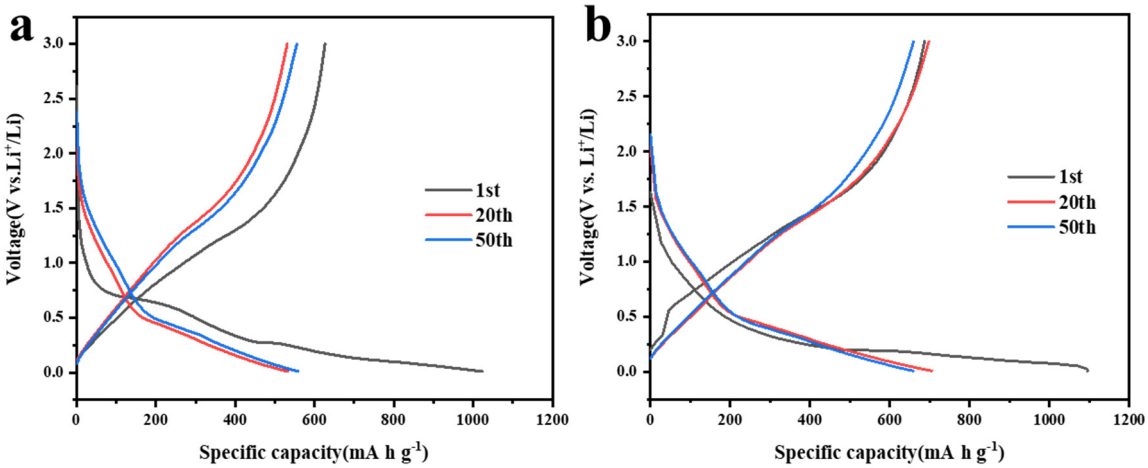


Figure 7. Discharge/charge curves in selected cycles for 5% MnO_2/CNFs (**a**) and 20% MnO_2/CNFs (**b**).

The cycle performances of 5% MnO_2/CNFs for 160 cycles and of 20% MnO_2/CNFs for 200 cycles at a current density of 0.1 A g^{-1} are shown in Figure 8a,b. The initial discharge/charge specific capacities of 20% MnO_2/CNFs are 1094 and 687 mA h g^{-1}, higher than those of 5% MnO_2/CNFs. As the cycles continue, the specific capacities 5% MnO_2/CNFs maintain at around 610 mA h g^{-1} from the 117th cycle to the 160th cycle, while those of 20% MnO_2/CNFs remain at around 835 mA h g^{-1} from the 133th cycle to the 200th cycle. During the whole process, their coulombic efficiency holds at around 98.9% and 99.5%, respectively; 20% MnO_2/CNFs owns the higher coulombic efficiency. The higher the percentage of MnO_2/CNFs, the better reversibility and structural stability [41–43].

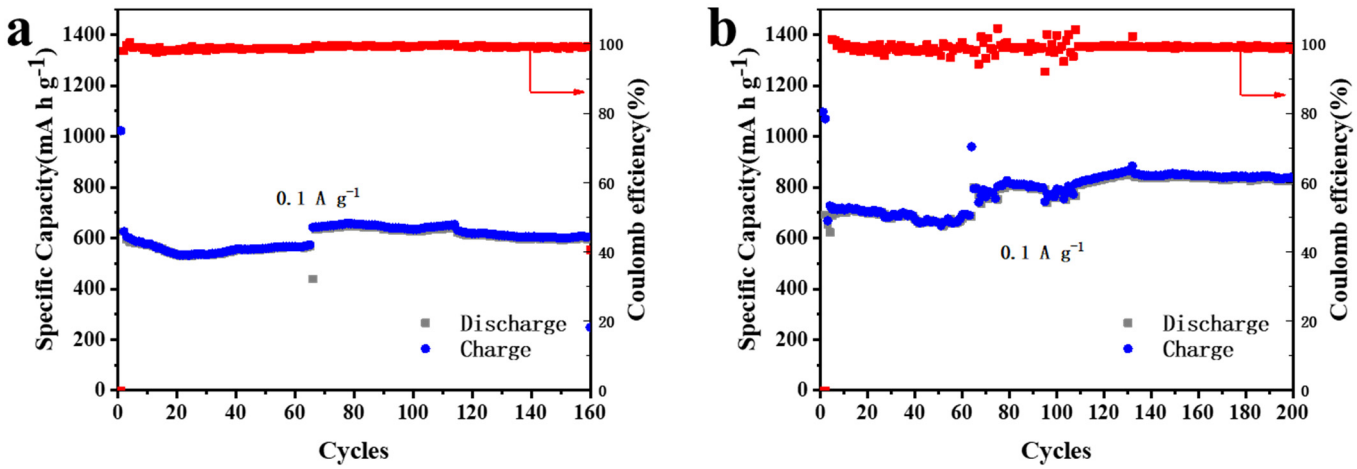


Figure 8. Cycling performance and coulombic efficiency of 5% MnO_2/CNFs for 160 cycles (**a**) and of 20% MnO_2/CNFs for 200 cycles (**b**) at a current density of 0.1 A g^{-1}.

To compare the discharge/charge capacity, the rate performances of MnO_2 NTs, 5% MnO_2/CNFs and 20% MnO_2/CNFs are tested at different current rates ranging from 0.1 to 0.5 A g^{-1} (Figure 9a–c). MnO_2 NTs do not contain the MnO_2/CNFs, so the structure is damaged easily and the cycle is unstable (Figure 9a). On the contrary, because of the carbon nanofibers, 5% MnO_2/CNFs and 20% MnO_2/CNFs have good structural stability (Figure 9b,c), but 20% MnO_2/CNFs show superior capacity, the corresponding invertible capacities are 796, 611, 552, 486 mA h g^{-1} at 0.1, 0.2, 0.3, 0.5 A g^{-1}. When tested again at 0.1,

0.2, 0.3 A g^{-1}, the reversible capacities of 835, 620,565 mA h g^{-1} are reached. In addition, the MnO_2/CNFs show better rate capability compared to the MnO_2 NTs nanoparticle electrode at different rates from 0.1 to 0.5 A g^{-1} (Figure 9) [44,45].

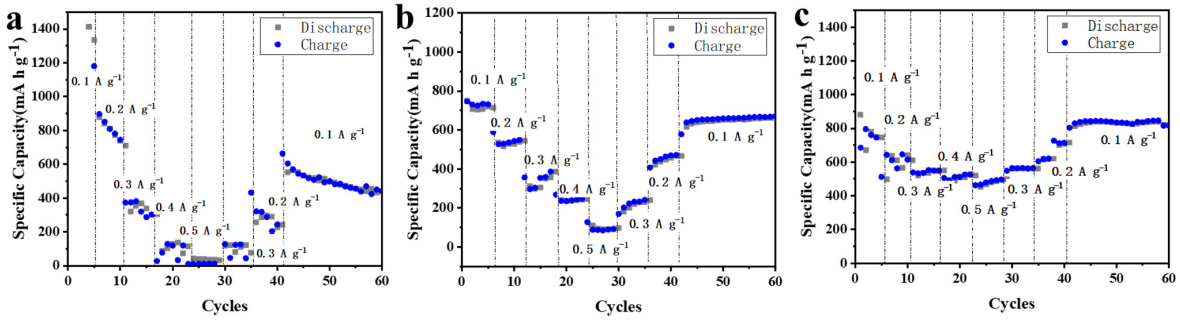


Figure 9. Rate performance of MnO_2 NTs (**a**), 5% MnO_2/ CNFs (**b**) and of 20% MnO_2/ CNFs (**c**) at various current rates ranging from 0.1 to 0.5 A g^{-1}.

To understand the state of the electrode process and the influence of mass transfer process based on the three different electrodes, EIS (electrochemical impedance spectra) were executed. As shown in Figure 10, the EIS of MnO_2 NTs, 5% MnO_2/CNF and 20% MnO_2/CNF are composed of semicircles and oblique lines, the high-middle frequency regions of the semicircles represent the charge transfer impedance of the electrode. The smaller the diameter of the arc, the lower the charge transfer impedance [46,47]. It is obvious that 5% MnO_2/CNF and 20% MnO_2/CNF have a smaller semicircle and the similar impedance values, indicating that both of them have a lower charge transfer impedance compared with MnO_2 NTs. The charge transfer resistances of MnO_2 NTs, 5% MnO_2/CNF and 20% MnO_2/CNF are 205, 245, and 495 Ω, respectively. The low frequency regions of the oblique lines are caused by the Warburg impedance of the ion diffusion; the larger the angle between the oblique line and the real axis, the better the ion diffusion of the capacitor, the higher electrochemical capacitance [35,46]. In Figure 10, the slope of the impedance lines of 5% MnO_2/CNF and 20% MnO_2/CNF is larger than that of MnO_2 NTs, and 5% MnO_2/CNF is the best of them, but the impedance semicircle of 5% MnO_2/CNF is rotated. The rotation of the impedance semicircle of 5% MnO_2/CNF is related to the inhomogeneity of the electrode/electrolyte interface. Because of the inhomogeneity of the electrode surface, the electrochemical activation energy of each point on the electrode surface may be different, which produces different charge transfer resistance values, leading to poor electrical conductivity [48,49]. To sum up, 20% MnO_2/CNF improves the conductivity on account of the unique structure with the carbon and has the best comprehensive performance.

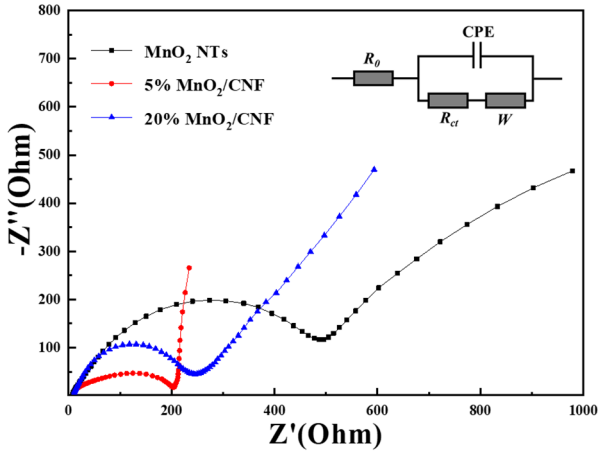


Figure 10. Electrochemical impedance spectra with selected equivalent circuit (inset) for MnO_2 NTs, 5% MnO_2/CNF and 20% MnO_2/CNF.

3.3. Analysis of Electrode Structure after Charge/Discharge

To further confirm the relationship between fiber structure and cycling stability, the electrode was disassembled after the cycling; the structure and morphology are shown in Figure 11. It may be very clearly seen that 20% MnO_2/CNFs still maintain the fiber structure, and the fiber structure is not broken. The structure of fiber can effectively release the expanded volume of the alloy during the lithium process, thus maintaining the structure stability and improving the stability and efficiency of the cycle.

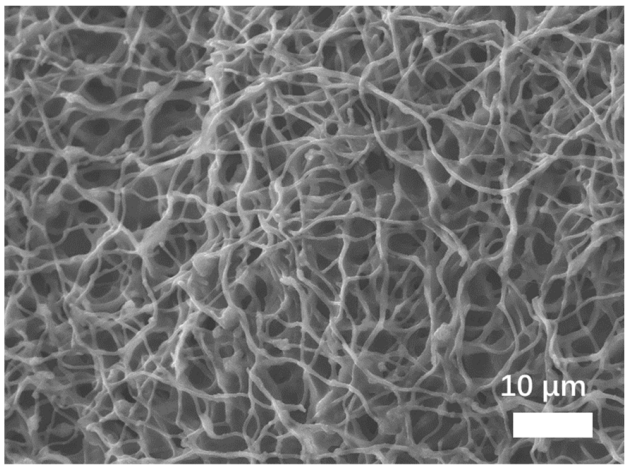


Figure 11. SEM images of the 20% MnO_2/CNFs after 200 cycles.

4. Conclusions

This study provides a simple method to prepare MnO_2/CNFs material as high-performance anode. MnO_2/CNFs were prepared by electrospinning, and the electrochemical properties of MnO_2 NTs, 5% MnO_2/CNFs and 20% MnO_2/CNFs were evaluated. SEM images proved that both of MnO_2/CNFs are the uniform nanofibers with a diameter of approximately 300–500 nm, which reveals that the uniform MnO_2/CNFs can be prepared. In comparison with them, 20% MnO_2/CNFs anode can provide the initial reversible capacity of 1094 mA h g^{-1} at 0.1 mA g^{-1} and remains at 835 mA h g^{-1} after 133 cycles. It is proved that the presence of CNFs improves the electrical conductivity of the composites by impedance spectrum. As a result, 20% MnO_2/CNFs had the better structural stability, high specific capacity, excellent reversibility, long cycling performance, and superior ionic conductivity, which provided ideas and prospect for designing a high-performance anode for LIBs.

Author Contributions: Conceptualization, D.M. and X.M.; methodology, M.Q.; software, D.M. and X.M.; validation, M.Q., X.Q. and G.Z.; formal analysis, D.M. and X.M.; investigation, D.M.; resources, M.Q.; data curation, D.M.; writing—original draft preparation, D.M.; writing—review and editing, D.M.; visualization, M.Q.; supervision, M.Q.; project administration, X.Q.; funding acquisition, M.Q. All authors have read and agreed to the published version of the manuscript.

Funding: The authors acknowledge financial support from Fundamental Research Funds for the Central Universities of Heilongjiang Province of China (2022-KYYWF-0603), Research Fund for the Doctoral Program of Higher Education of China (JMSUBZ 2020-02) and Fundamental Research Funds for the Central Universities of Heilongjiang Province of China (2021-KYYWF-0554).

Institutional Review Board Statement: Not applicable.

Informed Consent Statement: Not applicable.

Data Availability Statement: Not applicable.

Conflicts of Interest: The authors declare no conflict of interest.

References

1. Takeuchi, E.S.; Takeuchi, K.J.; Marschilok, A.C. The Ongoing Importance of Lithium Primary Batteries: 50+ Years and Going Strong. In *Electrochemical Society Meeting Abstracts 242*; The Electrochemical Society, Inc.: Pennington, NJ, USA, 2022; p. 102.
2. Zheng, Y.; Yao, Y.; Ou, J.; Li, M.; Luo, D.; Dou, H.; Li, Z.; Amine, K.; Yu, A.; Chen, Z. A review of composite solid-state electrolytes for lithium batteries: Fundamentals, key materials and advanced structures. *Chem. Soc. Rev.* **2020**, *49*, 8790–8839. [CrossRef]
3. Zeng, X.; Li, M.; Abd El-Hady, D.; Alshitari, W.; Al-Bogami, A.S.; Lu, J.; Amine, K. Commercialization of lithium battery technologies for electric vehicles. *Adv. Energy Mater.* **2019**, *9*, 1900161. [CrossRef]
4. Evarts, E.C. Lithium batteries: To the limits of lithium. *Nature* **2015**, *526*, S93–S95. [CrossRef]
5. Hu, Y.; Chen, W.; Lei, T.; Jiao, Y.; Huang, J.; Hu, A.; Gong, C.; Yan, C.; Wang, X.; Xiong, J. Strategies toward high-loading lithium–sulfur battery. *Adv. Energy Mater.* **2020**, *10*, 2000082. [CrossRef]
6. Roselin, L.S.; Juang, R.-S.; Hsieh, C.-T.; Sagadevan, S.; Umar, A.; Selvin, R.; Hegazy, H.H. Recent advances and perspectives of carbon-based nanostructures as anode materials for Li-ion batteries. *Materials* **2019**, *12*, 1229. [CrossRef] [PubMed]
7. Kour, S.; Tanwar, S.; Sharma, A. A review on challenges to remedies of MnO_2 based transition-metal oxide, hydroxide, and layered double hydroxide composites for supercapacitor applications. *Mater. Today Commun.* **2022**, *32*, 104033. [CrossRef]
8. Kamran, U.; Park, S.-J. Hybrid biochar supported transition metal doped MnO_2 composites: Efficient contenders for lithium adsorption and recovery from aqueous solutions. *Desalination* **2022**, *522*, 115387. [CrossRef]
9. Gu, X.; Yue, J.; Li, L.; Xue, H.; Yang, J.; Zhao, X. General synthesis of MnO_x (MnO_2, Mn_2O_3, Mn_3O_4, MnO) hierarchical microspheres as lithium-ion battery anodes. *Electrochim. Acta* **2015**, *184*, 250–256. [CrossRef]
10. Feng, L.; Xuan, Z.; Zhao, H.; Bai, Y.; Guo, J.; Su, C.-W.; Chen, X. MnO_2 prepared by hydrothermal method and electrochemical performance as anode for lithium-ion battery. *Nanoscale Res. Lett.* **2014**, *9*, 1–8. [CrossRef] [PubMed]
11. George, N.S.; Jose, L.M.; Aravind, A. *Review on Transition Metal Oxides and Their Composites for Energy Storage Application*; IntechOpen: London, UK, 2022.
12. Ashokkumar, K.; Dhanapandian, S.; Suthakaran, S.; Krishnakumar, N.; Anandan, M. Synthesis of MnO_2 nanoparticles and its effective utilization as high-performance of supercapacitor. *Mater. Today Proc.* **2022**, *49*, 2675–2678. [CrossRef]
13. Bach-Toledo, L.; Hryniewicz, B.M.; Marchesi, L.F.; Dall'Antonia, L.H.; Vidotti, M.; Wolfart, F. Conducting polymers and composites nanowires for energy devices: A brief review. *Mater. Sci. Energy Technol.* **2020**, *3*, 78–90. [CrossRef]
14. Voskanyan, A.A.; Ho, C.-K.; Chan, K.Y. 3D δ-MnO_2 nanostructure with ultralarge mesopores as high-performance lithium-ion battery anode fabricated via colloidal solution combustion synthesis. *J. Power Sources* **2019**, *421*, 162–168. [CrossRef]
15. Abdah, M.A.A.M.; Mokhtar, M.; Khoon, L.T.; Sopian, K.; Dzulkurnain, N.A.; Ahmad, A.; Sulaiman, Y.; Bella, F.; Su'ait, M.S. Synthesis and electrochemical characterizations of poly (3, 4-ethylenedioxythiophene/manganese oxide coated on porous carbon nanofibers as a potential anode for lithium-ion batteries. *Energy Rep.* **2021**, *7*, 8677–8687. [CrossRef]
16. Agobi, A.U.; Louis, H.; Magu, T.O.; Dass, P.M. A review on conducting polymers-based composites for energy storage application. *J. Chem. Rev.* **2019**, *1*, 19–34.
17. Sohal, N.; Maity, B.; Basu, S. Morphology effect of one-dimensional MnO_2 nanostructures on heteroatom-doped carbon dot-based biosensors for selective detection of glutathione. *ACS Appl. Bio Mater.* **2022**, *5*, 2355–2364. [CrossRef]
18. Mohammed, M.K.; Hassan, D.; Hashim, A. Exploring the optical properties of MnO_2 nanoparticles doped PVP for optoelectronics devices. *World J. Adv. Res. Rev.* **2023**, *17*, 1178–1185. [CrossRef]
19. Cui, Y.; Yang, K.; Lyu, Y.; Liu, P.; Zhang, Q.; Zhang, B. Hollow nitrogen-doped carbon nanofibers filled with MnO_2 nanoparticles/nanosheets as high-performance microwave absorbing materials. *Carbon* **2022**, *196*, 49–58. [CrossRef]
20. Sui, Y.; Liu, C.; Zou, P.; Zhan, H.; Cui, Y.; Yang, C.; Cao, G. Polypyrrole coated δ-MnO_2 nanosheet arrays as a highly stable lithium-ion-storage anode. *Dalton Trans.* **2020**, *49*, 7903–7913. [CrossRef]
21. Umar, A.; Ahmed, F.; Algadi, H.; Ibrahim, A.A.; Alhamami, M.A.; Qasem, H.; Akbar, S. Single crystalline α-manganese dioxide (α-MnO_2) nanowires as anode materials for lithium-ion batteries. *Mater. Express* **2022**, *12*, 1560–1565. [CrossRef]
22. Lin, Y.; Zhang, L.; Xiao, J.; Liu, H. MnO/C cubo-polyhedrons derived from α-MnO_2@ZIF-8 as anode materials for high-performance lithium-ion batteries. *Sustain. Energy Fuels* **2020**, *4*, 633–642. [CrossRef]
23. Cao, Z.; Yang, Y.; Qin, J.; Su, Z. A core-shell porous MnO_2/Carbon nanosphere composite as the anode of lithium-ion batteries. *J. Power Sources* **2021**, *491*, 229577. [CrossRef]
24. Sun, X.; Wang, J.; Huang, C.; Wu, Y.; Hou, J.; Situ, Y.; Huang, H. Electrochemical charge/discharge cycling and morphological effects in MnO_2/PANC nanostructures for supercapacitors. *Electrochim. Acta* **2022**, *428*, 140929. [CrossRef]
25. Ji, W.; Miao, X.; Zhang, T.C.; Wang, Y.; Yuan, S. Fe-metal-organic-framework/MnO_2 nanowire/granular activated carbon nanostructured composites for enhanced As (III) removal from aqueous solutions. *Appl. Surf. Sci.* **2022**, *606*, 155011. [CrossRef]
26. Kumar, R.R.; Thanigaivel, S.; Dey, N.; Priya, A.; Karthick, A.; Mohanavel, V.; Kannadhasan, S.; Muhibbullah, M.; Osman, S.M. Performance evaluation of cyclic stability and capacitance of manganese oxide modified graphene oxide nanocomposite for potential supercapacitor applications. *J. Nanomater.* **2022**, *2022*, 7352246. [CrossRef]
27. Shoukat, R.; Khan, M.I. Carbon nanotubes/nanofibers (CNTs/CNFs): A review on state of the art synthesis methods. *Microsyst. Technol.* **2022**, *28*, 885–901. [CrossRef]
28. Soltani, S.; Khanian, N.; Shojaei, T.R.; Choong, T.S.Y.; Asim, N. Fundamental and recent progress on the strengthening strategies for fabrication of polyacrylonitrile (PAN)-derived electrospun CNFs: Precursors, spinning and collection, and post-treatments. *J. Ind. Eng. Chem.* **2022**, *110*, 329–344. [CrossRef]

29. Li, C.; Bi, A.T.; Chen, H.L.; Pei, Y.R.; Zhao, M.; Yang, C.C.; Jiang, Q. Rational design of porous Sn nanospheres/N-doped carbon nanofibers as an ultra-stable potassium-ion battery anode material. *J. Mater. Chem. A* **2021**, *9*, 5740–5750. [CrossRef]
30. Azam, M.A.; Safie, N.E.; Ahmad, A.S.; Yuza, N.A.; Zulkifli, N.S.A. Recent advances of silicon, carbon composites and tin oxide as new anode materials for lithium-ion battery: A comprehensive review. *J. Energy Storage* **2021**, *33*, 102096. [CrossRef]
31. Zhang, N.; Yan, C.; Li, L.; Khan, M. Assessment of fiber factor for the fracture toughness of polyethylene fiber reinforced geopolymer. *Constr. Build. Mater.* **2022**, *319*, 126130. [CrossRef]
32. Zhao, X.; Zou, D.; Wang, S. Flexible phase change materials: Preparation, properties and application. *Chem. Eng. J.* **2022**, *431*, 134231. [CrossRef]
33. Zhang, X.; Su, X.; Zhang, B.; Wang, J. Preparation of MnO_2@ CNFs composites and their tunable microwave absorption properties. *Mater. Res. Express* **2019**, *6*, 075005. [CrossRef]
34. Wang, Z.; Han, Y.; Fan, W.; Wang, Y.; Huang, L. Shell-core MnO_2/Carbon@ Carbon nanotubes synthesized by a facile one-pot method for peroxymonosulfate oxidation of tetracycline. *Sep. Purif. Technol.* **2021**, *278*, 119558. [CrossRef]
35. Kim, E.S.; Lee, H.-J.; Kim, B.-H. Sandwich-structured carbon nanofiber/MnO_2/carbon nanofiber composites for high-performance supercapacitor. *Electrochim. Acta* **2022**, *406*, 139883. [CrossRef]
36. Huang, C.-L.; Chiang, L.-M.; Su, C.-A.; Li, Y.-Y. MnO_2/carbon nanotube-embedded carbon nanofibers as core–shell cables for high performing asymmetric flexible supercapacitors. *J. Ind. Eng. Chem.* **2021**, *103*, 142–153. [CrossRef]
37. Dirican, M.; Yanilmaz, M.; Asiri, A.M.; Zhang, X. Polyaniline/MnO_2/porous carbon nanofiber electrodes for supercapacitors. *J. Electroanal. Chem.* **2020**, *861*, 113995. [CrossRef]
38. Park, J.H.; Choi, W.Y.; Lee, S.; Kim, T.-S.; Lee, J.W. Graphene intercalated free-standing carbon paper coated with MnO_2 for anode materials of lithium ion batteries. *Electrochim. Acta* **2020**, *348*, 136310. [CrossRef]
39. Zhao, Y.; Chang, L.; He, W.; Xu, S.; Liu, K.; Huang, T.; Li, Y.; Cui, M.; Xie, J. Improved supercapacitive performances of manganese dioxide on acid-treated carbon nanofibers derived from polyaniline. *J. Energy Storage* **2023**, *60*, 106596. [CrossRef]
40. Yan, S.; Tang, C.; Wang, X.; Zhang, H.; Yang, Z.; Zhang, C.; Liu, S. Hierarchical MnO_2 nanowire arrays consisting of multitripod structures grown on porous carbon nanofibers for high-performance supercapacitor electrode. *J. Electroanal. Chem.* **2020**, *856*, 113475. [CrossRef]
41. Jeong, J.H.; Kim, Y.A.; Kim, B.-H. Electrospun polyacrylonitrile/cyclodextrin-derived hierarchical porous carbon nanofiber/MnO_2 composites for supercapacitor applications. *Carbon* **2020**, *164*, 296–304. [CrossRef]
42. Liu, C.-S.; Huang, C.-L.; Fang, H.-C.; Hung, K.-Y.; Su, C.-A.; Li, Y.-Y. MnO_2-based carbon nanofiber cable for supercapacitor applications. *J. Energy Storage* **2021**, *33*, 102130. [CrossRef]
43. Rao, T.P.; Kumar, A.; Naik, V.M.; Naik, R. Effect of carbon nanofibers on electrode performance of symmetric supercapcitors with composite α-MnO_2 nanorods. *J. Alloys Compd.* **2019**, *789*, 518–527. [CrossRef]
44. Yoon, J.; Choi, W.; Kim, T.; Kim, H.; Choi, Y.S.; Kim, J.M.; Yoon, W.-S. Reaction mechanism and additional lithium storage of mesoporous MnO_2 anode in Li batteries. *J. Energy Chem.* **2021**, *53*, 276–284. [CrossRef]
45. Ette, P.M.; Bosubabu, D.; Ramesha, K. Graphene anchored mesoporous MnO_2 nanostructures as stable and high-performance anode materials for Li-ion batteries. *Electrochim. Acta* **2022**, *414*, 140164. [CrossRef]
46. Ko, W.Y.; Sitindaon, R.S.; Lubis, A.L.; Yang, Y.R.; Wang, H.Y.; Lin, S.T.; Lin, K.J. Vertically-oriented zinc-doped γ-MnO_2 nanowalls as high-rate anode materials for li-ion batteries. *J. Energy Storage* **2022**, *54*, 105329. [CrossRef]
47. Huyan, Y.; Chen, J.; Yang, K.; Zhang, Q.; Zhang, B. Tailoring carboxyl tubular carbon nanofibers/MnO_2 composites for high-performance lithium-ion battery anodes. *J. Am. Ceram. Soc.* **2021**, *104*, 1402–1414. [CrossRef]
48. Liu, Z.; Li, X.; He, J.; Wang, Q.; Zhu, D.; Yan, Y.; Chen, Y. Is proton a charge carrier for δ-MnO_2 cathode in aqueous rechargeable magnesium-ion batteries? *J. Energy Chem.* **2022**, *68*, 572–579. [CrossRef]
49. Liu, Q.; Ma, C.; Qiao, W.; Ling, L.; Wang, J. Nanoarchitectured MnO_2 Confined to Mesoporous Carbon Microspheres as Bifunctional Electrodes for High-Performance Supercapacitors and Lithium-Ion Capacitors. *Ind. Eng. Chem. Res.* **2022**, *61*, 1748–1760. [CrossRef]

Disclaimer/Publisher's Note: The statements, opinions and data contained in all publications are solely those of the individual author(s) and contributor(s) and not of MDPI and/or the editor(s). MDPI and/or the editor(s) disclaim responsibility for any injury to people or property resulting from any ideas, methods, instructions or products referred to in the content.